

## $L_{23}$ - $MM$ Auger spectrum of $K$ -ionized argon: Decomposition by electron-ion and electron-electron coincidence techniques

U. Alkemper, J. Doppelfeld, and F. von Busch

*Physikalisches Institut, Universität Bonn, Nussallee 12, D-53115 Bonn, Germany*

(Received 27 May 1997)

The deexcitation cascade following photoionization of argon at energies above the  $1s$  threshold gives rise to a very complex  $L$ - $MM$  Auger spectrum extending from 100 to 230 eV. This spectrum consists of many overlapping  $L_{23}$ - $MM$  spectra, each of which is emitted in the presence of a different configuration of spectator vacancies left by preceding transitions. A prerequisite of a line analysis, therefore, is the decomposition of the observed spectrum into these partial spectra. A resolution of the Auger cascade into its parallel branches has been achieved by measuring in coincidence with the Auger spectrum the final ionic charge, whereas partial spectra emitted sequentially in the same cascade branch have been identified via electron-electron coincidence spectroscopy. The results are in very good agreement with those of a published step-by-step calculation of the cascade in relativistic single-configuration average. [S1050-2947(97)08410-2]

PACS number(s): 32.80.Hd, 32.50.+d, 32.90.+a

### I. INTRODUCTION

The Auger spectra of rare gases, as they are observed following electron-impact excitation, have for decades been prime examples of electron spectroscopy (see the review by Mehlhorn [1]). The best high-resolution spectra available today have been taken by Siegbahn and co-workers [2–4] more than 20 years ago and analyzed by them and others [5,6]. Recently, however, the subject has aroused interest as sources of intense and highly monochromatic synchrotron radiation, allowing well-specified primary excitation in the soft- and, more and more, also in the hard-x-ray regime, have become increasingly accessible. Thus Cooper *et al.* investigated the Auger spectrum of argon in the  $L_{23}$ - $MM$  energy range, employing photoexcitation at various energies up to just below the  $1s$  threshold. Thereby they were able to vary and separate the contribution of primary  $L_1$  ionization, which, after a Coster-Kronig vacancy transfer, gives rise to  $L_{23}M$ - $MMM$  emissions [7]. Alternative areas of research have been opened up such as the investigation of resonantly excited Auger spectra [8–12], the study and utilization of the Auger resonant Raman effect [13–15], and the analysis of the extremely complex Auger spectra emitted in later steps of the deexcitation cascade that follows deep core ionization [16]. Again the argon atom is a preferred target of study. Argon  $K$ - $LL$  and  $L$ - $MM$  spectra have been taken with monochromatic photoexcitation at the  $1s \rightarrow 4p$  resonance and at several energies above the  $1s$  ionization limit by Southworth *et al.* [17]. The experiments of this group concentrated upon coincidence measurements between  $K$ - $L$  fluorescence photons and electrons [18]. This technique was used to select the strong  $L_{23}$ - $M_{23}M_{23}$  transitions that were compared with Hartree-Fock calculations [19]. Furthermore, the same group investigated the angular correlation between the  $L_{23}$ - $M_{23}M_{23}$  electrons and  $K\alpha$  photons [20].

An attempt to analyze the full  $L$ - $MM$  spectrum observed after argon  $1s$  ionization has been made by von Busch *et al.* [16]. In their experiment the “white” beam of synchrotron radiation from a bending magnet ( $h\nu = 1.5$ – $10$  keV) was

used to excite the atoms. As compared to monochromatic excitation above the  $1s$  threshold, this approach provides a gain in photon flux by orders of magnitude. The observed  $L$ - $MM$  spectrum, however, is very similar and extends from 230 eV down to below 100 eV. Five groups of strong lines (one of which can be identified as largely representing the well-known  $L_{23}$ - $M_{23}M_{23}$  diagram transitions) are superimposed upon a quasicontinuous background of very many overlapping and weaker lines. It was shown that the spectrum is made up of more than half a dozen  $L_{23}$ - $MM$  spectra, each of which is emitted in the presence of a different configuration of “spectator” vacancies left by preceding Auger transitions. The additional holes change the screening of the electrons, thereby shifting the various partial spectra against each other. This leads to an overall structure of the compound spectrum, which was borne out by a step-by-step calculation of the cascade performed in single-configuration average by Günther and Hartmann [26]. A similar calculation showing comparable results has been published by Kochur and Sukhorukov [21]. The groups of intense lines mentioned above are mostly contributed by  $L_{23}$ - $M_{23}M_{23}$  transitions (the strongest ones) belonging to the prominent partial vacancy satellite spectra. Starting from here it was possible to assign the majority of the resolved lines emitted on the principal cascade branch ( $K$ - $L_{23}L_{23} \rightarrow L_{23}[L_{23}]-M_{23}M_{23}[L_{23}] \rightarrow L_{23}[M_{23}^2]-M_{23}M_{23}[M_{23}^2]$ ). A number of intermediate  $2p^5 3p^4$  ( $L_{23}^{-1}M_{23}^{-2}$ ) states have been energetically located [16].

Such an assignment of transition sequences, achieved with the aid of known initial  $2p^4$  and final  $3p^2$  levels, could not be extended to other principal (i.e.,  $K$ - $L_iL_k$ ) cascade branches because here the necessary auxiliary data are not available. Thus, while the overall intensity distribution of the observed spectrum is consistent with the result of the calculation by Günther and Hartmann, it was not possible to push the experimental analysis of the general spectral structure and, based on it, the identification of transitions any further. Inspection of the cascade diagram, however, shows that (when double electron ejections are disregarded) each prin-

cipal branch leads to a final ion of a specific charge and that in most branches two  $L_{23}$ - $MM$  transitions occur in sequence. Therefore, electron spectroscopy in coincidence with a charge analysis of the final ion decomposes the spectrum into the cascade branches, whereas electron-electron coincidence spectroscopy identifies partial spectra emitted within one and the same branch. Such electron-ion and electron-electron coincidence studies are the subject of the present work. As will be seen, they reveal the spectral composition completely albeit at low resolution. Individual transitions shall be dealt with elsewhere, where the line analysis given by von Busch *et al.* [16] is planned to be refined and complemented by a relativistic calculation of energies and intensities [22].

## II. EXPERIMENT

With respect to the excitation and noncoincident measurement of the spectrum, the experimental setup has been described before [16]. Those measurements, as well as the ones to be presented here, were performed at the electron accelerator ELSA at Bonn, which was operated at 2.3 GeV electron energy in storage mode. The white x-ray beam from a bending magnet was filtered by a 125- $\mu\text{m}$  Be and, for some of the data taken, an additional 25- $\mu\text{m}$  polyamide (Kapton, DuPont) window. Photoabsorption has been calculated to take place between 1500 and 8000 eV and leads to primary ionization at the  $K$ ,  $L_1$ , and  $L_{23}$  shells in approximate proportions of 1:0.19:0.15 [16]. For comparison, monochromatic photoexcitation above the  $1s$  threshold would cause only about 9% primary  $L$  ionization, but in any case some 12% of the initial  $K$  holes are transferred to the  $L_{23}$  shell by  $K\alpha$  fluorescence. As expected then, a somewhat reduced intensity in the regions of the  $L_{23}$ - $MM$  and  $L_{23}M$ - $MMM$  partial spectra indeed is observed when the spectrum is taken with monochromatic photoexcitation [17,18], as compared to broadband irradiation [16]. However, the undispersed x-ray beam is more intense by orders of magnitude.

The noncoincident electron spectrum was taken at 0.45 eV resolution with a rotationally symmetric spectrometer (MAC 2, Riber) resembling in geometry a double-pass cylindrical mirror analyzer (CMA) but employing retardation [23]. The instrument was oriented perpendicularly to the accelerator plane. We have remeasured the  $L_{23}$ - $MM$  spectrum in the energy range between 172 and 228 eV with a somewhat improved resolution of 0.35 eV, but in the present work shall use as a reference the spectrum published before [16] because of its larger energy range. In addition to the broadband photoexcited spectrum we have also recorded an  $L_{23}$ - $MM$  spectrum at 0.35-eV resolution after excitation with 3-keV electrons.

For the electron-ion coincidence experiment the electron spectrometer was combined coaxially with a time-of-flight mass spectrometer. Detection of an electron of the selected energy provides the start signal for the time measurement. Ions are detected by a multichannelplate tandem at a potential of 5 kV. It is assumed that the overall detection probability ( $>0.37$ ) is independent of the ionic charge. This assumption is supported by the observation that the ratio of true electron-ion coincidences over electron counts does not vary with electron energy [and hence with the average ionic charge; cf. Fig. 4(b)] by more than  $\pm 10\%$  between 170 and

210 eV. The variations show no correlation with the ionic charge but rather with the coincident count rate, thereby indicating that the relative contribution of spurious electrons from surfaces, etc., changes with the Auger spectral intensity. A static electric field of 14 V/mm was applied to extract the ions. The undispersed x-ray beam is collimated in the direction of the spectrometer axis to a height of 0.2 mm. With the  $\Delta E$  of the electron spectrometer set at 4 eV, the effective energy resolution then is 5 eV. We used a target pressure of  $5 \times 10^{-6}$  mbar. A more detailed description of the experimental setup can be found elsewhere [24]. Coincidence rates were 20 Hz at maximum.

Electron-electron coincidence spectra were taken using the MAC 2 spectrometer and a modified single-pass CMA with preretardation and a large steric angle of  $0.075 \times 4\pi$  (ESA 150, Staib Instrumente). Both instruments are mounted opposite to each other with a common vertical axis. They are positioned independently for maximum noncoincident count rates, the coincidence rate itself being too low for alignment. The photon beam is being monitored via electron emission from a steel cylinder serving as a beam dump.

Output pulses from the channeltron detectors of the spectrometers are amplified, discriminated, and fed to the start and, via a delay, the stop input, respectively, of a time-to-digital converter of 1-ns resolution. Time histograms were recorded repeatedly over short periods ( $\approx 1$  min) determined by a constant integrated signal from the photon monitor. The time delay spectrum shows a peak of true coincidences superimposed upon a continuous background of random ones, which was determined as follows. The rate of random coincidences is proportional to the product of the noncoincident pulse rates of the two spectrometers. For reasons of better statistics the proportionality constant was obtained from the sum of all time histograms taken irrespectively of the selected electron energy (the shift of the "true" peak with energy is insignificant). For each histogram then the expected background of random coincidences was calculated from the noncoincident rates and subtracted to give the true coincidence count. At an x-ray flux of  $2 \times 10^{12}$  equivalent photons/s (referred to as the  $K$  edge), a target density of about  $3 \times 10^{13}$   $\text{cm}^{-3}$  and bandpasses of 4 eV for the MAC 2 and 10 eV for the ESA spectrometer, the noncoincident rates are a few kilohertz and the rate of true coincidences 0.6 Hz at maximum.

Calibration of the electron spectra was performed by comparison with the electron impact excited high-resolution  $L$ - $MM$  spectrum of argon taken by Werme *et al.* [3]. Energy positions were derived from fitting, after subtraction of an estimated background, Gaussians to observed lines. Our electron-impact-excited spectrum was calibrated by a linear regression of the lines 32, 45, 72, and 78 in the numbering of Werme *et al.* to the energies quoted by these authors. The deviations were below 0.02 eV. The  $L_{23}$ - $MM$  satellite spectrum measured with broadband photoexcitation [16] was recalibrated in a similar way by means of lines 32, 45, 48, 52, 60, 72, and 75–77, which can be recognized also in this much more densely populated spectrum. The calibration error is estimated to be 0.07 eV. Calibration of the coincidence spectra finally has been achieved by comparison of the noncoincident spectrum, recorded under the experimental conditions of the respective coincidence experiment, with the

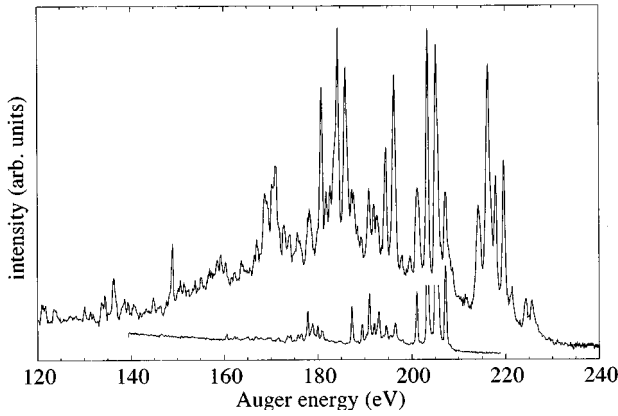


FIG. 1.  $L_{23}$ - $MM$  Auger spectrum of argon emitted after broadband photoexcitation at energies above the  $K$  edge [16] (top) and  $L_{23}$ - $MM$  Auger spectrum of argon as excited by impact of 3-keV electrons (bottom).

high-resolution photoexcited one [16] convolved with a Gaussian of appropriate width. We estimate a calibration error of 0.3 eV for the electron-ion coincidence spectrum and of 0.17 eV for the electron-electron coincidence spectra.

### III. RESULTS AND DISCUSSION

The  $L_{23}$ - $MM$  spectrum recorded by von Busch *et al.* after broadband photoexcitation at an energy resolution of about 0.45 eV [16] is displayed in Fig. 1. This spectrum is very similar to the one measured by Southworth *et al.* [17,18], which was excited by 3211.3-eV photons, i.e., 5 eV above the  $1s$  ionization limit. In either case the major part of absorption leads to  $K$  ionization. Hence most of the spectrum is contributed by  $L$ - $MM$  transitions representing later steps in a deexcitation cascade and therefore taking place in the presence of additional, spectator vacancies. The various branches of the cascade are depicted in Fig. 2, where the states are represented in an independent-particle approximation, i.e., as single configurations of vacancies. Three main branches are seen starting from a primary  $K$  hole and in each of them two  $L_{23}$ - $MM$  transitions occur sequentially and in the presence of different configurations of spectator vacancies. In addi-

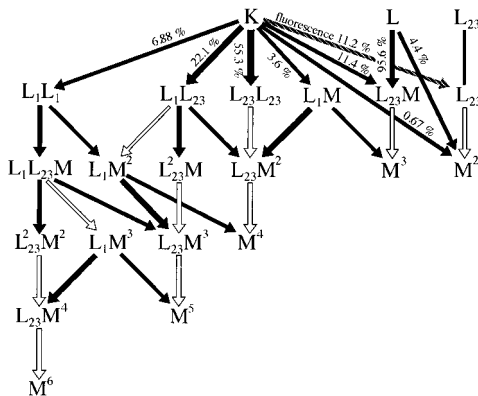


FIG. 2. Schematic representation of the vacancy configurations and the transitions arising in the deexcitation of primary  $K$ ,  $L_1$ , and  $L_{23}$  holes. White arrows signify the various  $L_{23}$ - $MM$  vacancy satellite transitions. The indicated branching ratios have been taken from [28].

tion, there are the branches starting from a single initial  $L_1$  or  $L_{23}$  hole, which give rise to the  $L_{23}M$ - $MMM$  and the ordinary  $L_{23}$ - $MM$  spectrum, respectively. It is evident that there exists a considerable variety of vacancy configurations acting as spectators to an  $L_{23}$ - $MM$  transition. Each of these vacancy configurations gives rise to an entire  $L_{23}$ - $MM$  spectrum of its own. (Henceforth we shall denote the various partial  $L_{23}$ - $MM$  spectra by the configuration of spectator holes set in square brackets, e.g.,  $L_{23}[M^2]$ - $MM[M^2]$  or simply  $[M^2]$ . A similar notation, indicating the active electrons and the spectator holes, will be used to label the transition multiplets while individual levels will be given in orbital notation.) These partial spectra overlap each other and are expected, with the exception of those lying in the  $K$ - $L_1L_1$  branch, to contribute on the same order of integrated intensity to the compound spectrum of Fig. 1 [16]. This explains why the latter shows, notably in comparison to the electron-impact-excited  $L_{23}$ - $MM$  spectrum (Fig. 1), such a wealth of lines, which obviously are largely unresolved. Any assignments of transitions therefore have to be preceded by an analysis of the gross spectral structure.

The occurrence of distinct groups of intense lines (Fig. 1) suggests that the partial spectra lie separated in energy at least to a first approximation, and indeed this has been shown to be the case [16]. The partial spectra are expected to resemble each other in overall structure, which roughly can be taken from the electron-impact-excited spectrum dominated by the  $L_{23}$ - $MM$  diagram lines (Fig. 1). As the multiplet splitting is smaller than the  $M_1$ - $M_{23}$  binding energy difference of about 15 eV, each partial  $L_{23}$ - $MM$  spectrum consists, in decreasing order of energy and intensity, of three groups of lines representing the  $L_{23}$ - $M_{23}M_{23}$ ,  $L_{23}$ - $M_1M_{23}$ , and  $L_{23}$ - $M_1M_1$  transition multiplets, respectively. In fact, the last group is rather weak and interspersed with correlation satellites [3,5]. Differences between the spectra exist in two respects: The line splitting within the multiplet groups is modified by coupling to the angular momenta of the additional holes and, moreover, the spectator vacancies cause, by a change of the electrostatic screening, an overall energetic shift [25]. It is these various specific shifts together with the group subdivision of each partial spectrum that determine the gross structure of the observed compound  $L$ - $MM$  spectrum.

For the case of argon the energy shifts have been determined by Günther and Hartmann, who calculated the entire cascade step by step in a relativistic single-configuration approximation, neglecting multiplet splitting and shake processes [16,26]. They found that an  $L$  spectator hole increases the average  $L_{23}$ - $MM$  transition energy by 10 eV, whereas a decrease of about 10 eV was obtained per  $M$  spectator vacancy. The calculation starts from a distribution of primary  $K$ ,  $L_1$ , and  $L_{23}$  holes that approximates the one generated by the broadband photoexcitation employed in the experiment. The resulting gross distribution of the superimposed  $L_{23}$ - $MM$  spectra is shown in Fig. 4(c) where we have convolved the theoretical bar spectrum with a Gaussian of a width [4 eV full width at half maximum (FWHM)] chosen arbitrarily to give a rough indication of the actual multiplet splitting. It is seen that the theoretical overall intensity distribution quite well matches the gross observed one, except in the low-energy part of the spectrum where shake and correlation satellites are expected to lie, which were neglected in

the calculation. Specifically, the prominent groups of lines present in the experimental spectrum appear to be identifiable with strong  $L_{23}\text{-}M_{23}M_{23}$  transition multiplets belonging to various spectator hole configurations. With respect to the further analysis, two observations are to be noted: The  $L_{23}[L_{23}]\text{-}M_{23}M_{23}[L_{23}]$  group, emitted in the presence of a single  $L_{23}$  spectator vacancy, is the only one shifted towards higher energies against the  $L_{23}\text{-}M_{23}M_{23}$  diagram lines, thus being rather free from contaminations by other spectra. Moreover, partial spectra emitted sequentially in the same cascade branch (cf. Fig. 2) are shifted against each other by some 30 eV and hence have comparatively little overlap. These circumstances have been exploited for the analysis of individual spectral lines emitted in the principal  $K\text{-}L_{23}L_{23}$  branch of the cascade [16].

That investigation, resulting in the identification of pairs of lines emitted in sequence, lends strong support to the calculated gross spectral structure as far as the intense  $L_{23}\text{-}M_{23}M_{23}$  groups belonging to the most probable deexcitation branch are concerned. A more comprehensive test of the calculation, not restricted to isolated prominent lines, is provided by electron-ion coincidence measurements. As can be read from Fig. 2, each branch of the electronic deexcitation finally leads to an ion of a specific charge, at least as long as double electron ejections are disregarded. The  $K\text{-}LL$  principal cascade branches each contain two  $L_{23}\text{-}MM$  partial spectra, but these, as we have seen, are expected to be well separated in energy. Thus a measurement of the entire  $L_{23}\text{-}MM$  spectrum in coincidence with a charge analysis of the final ion should yield a complete decomposition into the partial vacancy satellite spectra.

We have performed such an experiment, determining branching ratios for ions of charge  $q=2\text{--}8$ . Time-of-flight spectra were taken for a whole series of pass energies of the electron spectrometer at increments of 1–2 eV. The bandpass was set at 4 eV, but the effective energy resolution is 5 eV due to the presence of the static electric field. Figure 3 shows a few of the raw time-of-flight spectra, all normalized to equal height of the largest peak. The change of the spectra with the energy of the electron detected in coincidence is readily apparent. Each spectrum contains more than one charge peak, thus directly demonstrating the overlap of the partial spectra.  $\text{Ar}^{7+}$  (<5%) and  $\text{Ar}^{8+}$  (<1%) are present, but shall be neglected in the following.  $\text{Ar}^{1+}$ , though having been detected at a low level after monochromatic photoexcitation at energies below and above the  $K$  edge [27], was found to be missing. A small constant ionic background resulting from trigger electrons without temporal correlation to the ions amounts at most to about 1% of the peak integrals and has been subtracted. The broadband excitation causes a smooth and nearly constant background of  $K$  photoelectrons in the Auger spectrum, which can be estimated to give roughly 3% of the integral intensity and should in coincidence lead to a discrete ion time-of-flight spectrum similar to the one that has been measured for monochromatic photoexcitation at 3400 eV by Doppelfeld *et al.* [27]. Indeed, at 242-eV electron energy, where no Auger peaks are seen anymore, the coincident count rate is about 5% of that observed in the energy range of the strong line groups and the coincident ion spectrum shows all charges from 2 to 7 (Fig. 3). Their intensity distribution agrees reasonably with expecta-

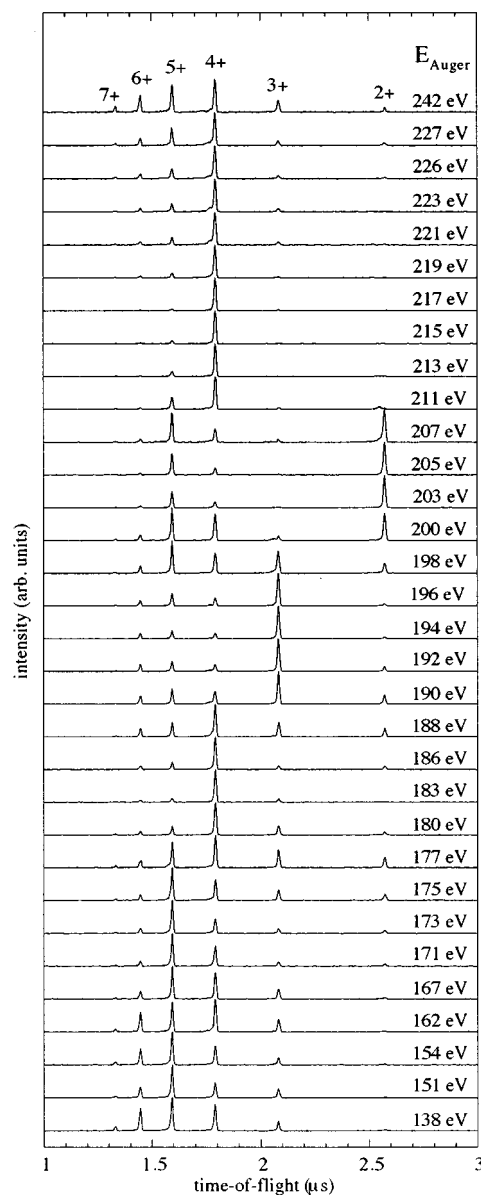


FIG. 3. Ion time-of-flight spectra taken in coincidence with electrons of selected energies indicated in the figure. All spectra are normalized to equal height of the strongest peak.

tion and with the one obtained by summing the time-of-flight spectra of Fig. 3 over electron energy. No correction has been applied for this type of background.

Branching ratios of the various ionic charges were determined by integration of the peaks in the time-of-flight spectra. Thereafter the sum was normalized at each electron energy to the noncoincident electron spectrum measured under the conditions of the electron-ion coincidence experiment. The resulting ion-charge-resolved electron spectra are displayed in Fig. 4(b). It is seen that the theoretical prediction of Fig. 4(c) is confirmed in all essential traits and to a high degree also quantitatively. Note, however, that in its original form this prediction was given as a bar spectrum [16], which we have convolved with a Gaussian of arbitrary width, whereas the experiment gives the true spectral distribution, albeit at rather low resolution. In principle, it is possible by way of electron-ion coincidence measurements to assign the

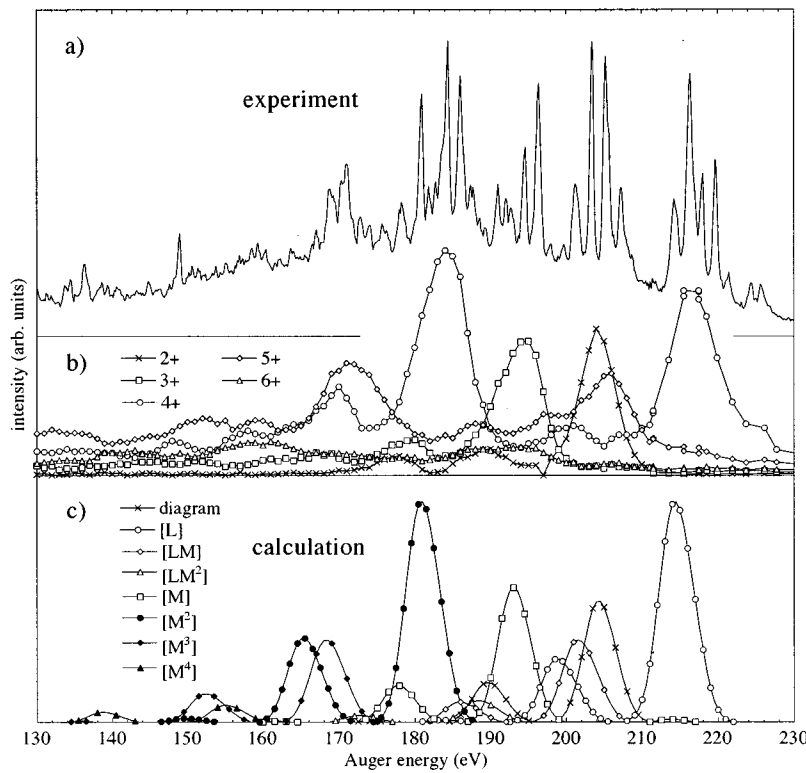


FIG. 4. (a)  $L_{23}$ - $MM$  Auger spectrum observed noncoincidentally after broadband photoexcitation [16]; (b) spectral distribution of  $L_{23}$ - $MM$  electrons observed in coincidence with final ions of charges 2–6; and (c) transition multiplets of the partial  $L_{23}$ - $MM$  spectra, emitted in the presence of various spectator vacancy configurations as indicated (calculated bar spectrum [16] convolved with a Gaussian of 4 eV FWHM).

spectrum line by line to the spectator hole configurations.

The calculated principal structure of each partial spectrum, consisting of a strong high-energy group of  $L_{23}$ - $M_{23}M_{23}$  lines accompanied by a weaker  $L_{23}$ - $M_1M_{23}$  one at some 15-eV lower energy, is clearly reproduced for charges  $q=2-5$ . In addition, there is, for every ionic charge  $q>2$ , a low-energy tail of intensity extending all the way down to 130 eV and doubtless beyond. This tail is attributed to correlation satellites and to shakeoff, which were not included in the theoretical treatment. In accordance with this interpretation, all charges  $q>3$  are found here above the background level, whereas the calculation predicts only  $q=5$  and 6.

We now shall discuss the partial spectra as they appear in coincidence with individual ionic charges.  $Ar^{2+}$  ions arise from  $L_{23}$  ionization and a subsequent  $L_{23}$ - $MM$  transition, but in the present experiment  $L_{23}$  holes are generated at a comparable rate also via  $K$  ionization and  $K\alpha$  fluorescence (cf. Fig. 2). Since electron-impact ionization takes place predominantly at the  $L_{23}$  shell, the Auger spectrum observed in coincidence with  $Ar^{2+}$  ions is similar to the electron-impact-excited one. The comparison is displayed in Fig. 5, where in addition Gaussian peaks indicating the calculated intensities of the  $L_{23}$ - $M_{23}M_{23}$ ,  $L_{23}$ - $M_1M_{23}$ , and  $L_{23}$ - $M_1M_1$  transition multiplets [16] are shown. Three peaks are also seen at the low resolution of the coincidence experiment, corresponding to three groups of lines appearing in the electron-impact-excited spectrum. The second maximum of the coincidence spectrum falls at a somewhat lower energy than the bulk of the associated electron-impact-excited lines. This energy

shift is only apparent though since quite a few of these lines between 190 and 197 eV have been ascribed to  $L_{23}[M]$ - $MM[M]$  transitions [3,5] and do not cause coincidences with  $Ar^{2+}$  ions. However, the integral intensity of the second coincidence peak (like that of the corresponding group of electron-impact-excited lines) is, in relation to the  $L_{23}$ - $M_{23}M_{23}$  maximum, somewhat below the theoretical prediction, whereas the low-energy peak of the coincidence spectrum far exceeds the calculated strength of the

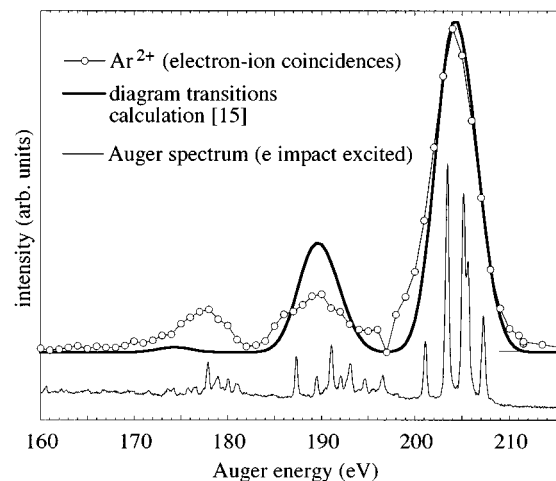


FIG. 5.  $L_{23}$ - $MM$  Auger spectrum observed in coincidence with  $Ar^{2+}$  ions, compared with the calculation [16] [cf. Fig. 4(c)] and the electron-impact-excited  $L_{23}$ - $MM$  spectrum. The  $L_{23}$ - $M_{23}M_{23}$  peaks of the former two spectra have been normalized to equal height.

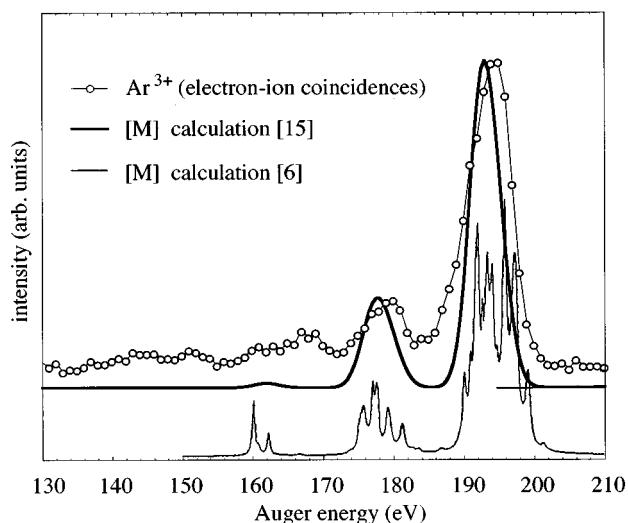


FIG. 6.  $L_{23}$ - $MM$  Auger spectrum observed in coincidence with  $\text{Ar}^{3+}$  ions, compared with the calculated  $L_{23}[M]$ - $MM[M]$  “Gaussian” spectrum [16] [cf. Fig. 4(c)] and the semiempirical high-resolution  $L_{23}$ - $MM$  “transfer” spectrum of Cooper *et al.* [7]. The  $L_{23}$ - $M_{23}M_{23}$  peaks of the former two spectra have been normalized to equal height.

$L_{23}$ - $M_1M_1$  transitions. Indeed, the corresponding group of lines, appearing around 180 eV in the electron-impact-excited spectrum, is dominated by correlation satellites (not included in the calculation) of final configurations  $3s^23p^3(^2P)(4s,3p,3d)$  and  $3s^23p^3(^2D)(3d,4d)$  [3], while the line doublet identified as  $L_{23}$ - $M_1M_1$  is very weak [5].

$\text{Ar}^{3+}$  ions arise chiefly from primary  $L_1$  holes that are transferred by a fast  $L_1$ - $L_{23}M$  Coster-Kronig transition to the  $2p$  subshell. Some  $L_{23}M$  double vacancies are generated also through  $K$  ionization followed by a  $K$ - $L_{23}M$  transition (Fig. 2) and through direct double photoionization. The final Auger step is an  $L_{23}$ - $MM$  emission in the presence of an  $M$  spectator vacancy. The pertinent partial spectrum is observed weakly also after electron-impact excitation, and quite a number of lines has been assigned to it [3,5]. It has been further investigated in some detail by Cooper *et al.* [7], who compared experimental electron spectra excited by 2000-eV electrons with similar ones excited by 2200-eV and 3174-eV photons. Taking advantage of the fact that the ratio of primary  $L_1$  to  $L_{23}$  holes increases with photon energy, the authors tried to isolate the  $L_{23}[M]$ - $MM[M]$  “transfer” spectrum from the “normal”  $L_{23}$ - $MM$  one with the help of semiempirical calculations. Although the high line density did not allow them to identify specific observed lines with calculated transitions, the general distribution of the calculated spectrum is in accordance with the experiment. Figure 6 shows this calculated transfer spectrum [7] together with our  $\text{Ar}^{3+}$  coincident one and with the result of the cascade calculations [16]. Similar to the case of the normal spectrum (Fig. 5), we see in the coincidence spectrum a strong peak (at 195 eV), which can be assigned to the  $L_{23}[M]$ - $M_{23}M_{23}[M]$  transitions, and a weaker one around 180 eV, representing the  $L_{23}[M]$ - $M_1M_{23}[M]$  transitions. The remainder of the coincident intensity appears to be a broad distribution of shake and correlation satellites extending from 170 eV down to less than 130 eV. It is not possible to locate the calculated

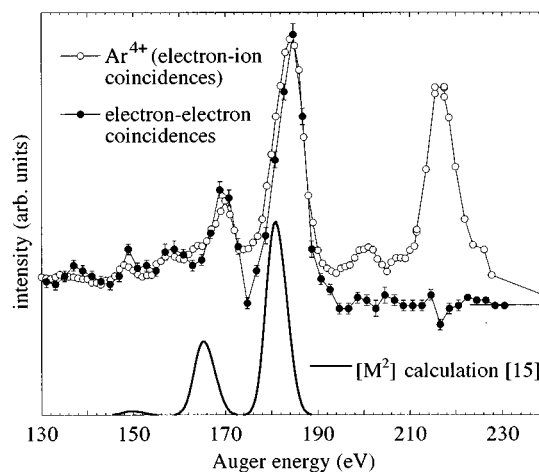


FIG. 7.  $L_{23}$ - $MM$  Auger spectrum observed in coincidence with  $\text{Ar}^{4+}$  ions and with electrons of  $215.5 \pm 5$  eV, respectively. For comparison, also the calculated  $[M^2]$  vacancy satellite spectrum [16] [cf. Fig. 4(c)] is displayed.

$L_{23}[M]$ - $M_1M_1[M]$  group in this distribution, and indeed the final states of these transitions are expected to be subject to strong configuration mixing like the corresponding ones in the normal  $L_{23}$ - $MM$  spectrum [5,6]. A comparison between individual lines observed in the compound vacancy satellite spectrum with those appearing in the electron-impact-excited one shall be given elsewhere [22].

$\text{Ar}^{4+}$  ions play a negligible role in electron-impact experiments as they are generated only via  $K$  excitation. 84% of the  $K$  holes [28] decay by a  $K$ - $LL$  transition, which is followed by two  $L_{23}$ - $MM$  emissions. Thus each of the final charges  $q=4-6$  is observed in coincidence with two partial  $L_{23}$ - $MM$  spectra belonging to different spectator hole configurations and therefore separated in energy. For the most intense cascade branch, leading via a  $K$ - $L_{23}L_{23}$  emission to final  $\text{Ar}^{4+}$  ions, it has been shown by direct identification that almost all lines in the prominent groups around 215 eV and 185 eV (Fig. 1) can be combined to pairwise sequential transitions of the type  $2p^4$ - $2p^53p^4$ - $3p^2$  [16]. The remaining regions of the two partial spectra involved (i.e., the  $L_{23}[L_{23}]$ - $MM[L_{23}]$  and  $L_{23}[M^2]$ - $MM[M^2]$  ones) are heavily overlapped by other spectra, as can be seen in Fig. 4. We have tried to separate them not only by electron-ion but also by electron-electron coincidence spectroscopy, the results of which shall be presented now.

Searching for transitions occurring in the final  $L_{23}[M^2]$ - $MM[M^2]$  step, we fixed the bandpass of the ESA spectrometer at 10 eV width upon the group of  $2p^4(^1D_2)$ - $2p^53p^4$  lines, which represent the strongest part of the  $L_{23}[L_{23}]$ - $MM[L_{23}]$  spectrum. Adjusting for maximum intensity, the center of this “coincidence window” was set at  $215.5 \pm 2$  eV. The bandpass of the MAC spectrometer was chosen at 4 eV FWHM and its center stepped through the energy range from 130 to 230 eV, while at each energy a time delay distribution of coincidence events was taken from which we derived the rate of true coincidences. The resulting electron-electron coincidence spectrum is displayed in Fig. 7, together with the Auger spectrum measured in coincidence with  $\text{Ar}^{4+}$  ions and the calculated  $[M^2]$  spectrum [16], respectively.

The double-peak structure predicted for each of the partial spectra involved is quite well reproduced by the electron- $\text{Ar}^{4+}$  coincidence rate, although we note energy shifts of 3–4 eV between experiment and theory. We thus assign the peaks at 215, 200, 185, and 170 eV to  $L_{23}[L_{23}]-M_{23}M_{23}[L_{23}]$ ,  $L_{23}[L_{23}]-M_1M_{23}[L_{23}]$ ,  $L_{23}[M^2]-M_{23}M_{23}[M^2]$ , and  $L_{23}[M^2]-M_1M_{23}[M^2]$  transitions, respectively. The electron-electron coincidence measurement gives essentially zero intensity at energies greater than 195 eV. This is expected since the energy difference between the  $2p^4(^1D_2)$  and the lowest  $3p^2$  state is 402.7 eV [16] and the transitions falling into the coincidence window have energies greater than about 205 eV. At energies below 190 eV the two coincidence spectra agree very well with each other, thereby proving the sequential emission of the  $[L_{23}]$  and  $[M^2]$  partial spectra. However, even below 190 eV the two coincidence spectra contain not exactly the same transitions. The electron-electron coincidence window around  $215.5 \pm 5$  eV brackets, besides the  $2p^4(^1D_2)-2p^53p^4$  lines, also transitions that lead to final  $\text{Ar}^{5+}$  ions and belong to the  $[L_{23}M]$  partial spectrum. Their share is estimated with the help of the data shown in Fig. 4(b) to be about 16%. According to the calculations,  $L_{23}-M_{23}M_{23}$  lines of the subsequently emitted  $[M^3]$  spectrum appear around 170 eV, where indeed the electron- $\text{Ar}^{5+}$  coincidences exhibit a strong peak. A minor fraction of the intensity seen in the electron-electron coincidence peak at 170 eV therefore is due to coincidences between  $L_{23}[L_{23}M]-MM[L_{23}M]$  and  $L_{23}[M^3]-M_{23}M_{23}[M^3]$  electrons. The peak at 185 eV in the electron- $\text{Ar}^{4+}$  coincidence spectrum contains mainly  $L_{23}[M_{23}^2]-M_{23}M_{23}[M_{23}^2]$  but also  $L_{23}[M_1M_{23}]-M_{23}M_{23}[M_1M_{23}]$  transitions, whereas the latter do not contribute to the corresponding electron-electron coincidence peak since the precursor  $L_{23}[L_{23}]-M_1M_{23}[L_{23}]$  transitions fall around 200 eV and thus outside the coincidence window.

The electron- $\text{Ar}^{4+}$  coincidence signal below 160 eV is due to the  $L_{23}[M^2]-M_1M_1[M^2]$  transitions, correlation satellites of the  $[M^2]$  lines, and  $[M]$  transitions accompanied by shakeoff. The electron-electron spectrum may contain here additional contributions of  $[M^3]$  transitions, but shows structure very similar to that of the electron- $\text{Ar}^{4+}$  coincidence spectrum. Interestingly, the maximum at 149 eV coincides with a conspicuous narrow peak in the noncoincident spectrum at 149.11 eV (Fig. 1). According to a multiconfiguration Dirac-Fock calculation [22], there exists at about this energy a comparatively intense transition belonging to the  $[M_{23}^2]$  spectrum, namely, the line  $[2p^5(^2P)3p^4(^1D)]^2F_{7/2}-3s^03p^4(^1D_2)$ . As the final state shows excessive configuration mixing to the extent of a complete breakdown of the orbital picture, the transition energy is difficult to determine precisely, but the line is by far the dominant one predicted in this energy range.

The relative intensities of the  $[M^2]$  spectrum contained in the electron-electron coincidence peaks at 185 and 170 eV and in the low-energy tail can be estimated after correcting for coincidences between  $[LM]$  and  $[M^3]$  transitions with the help of the electron-ion coincidence data. We find the following figures: 175–193 eV, 56%; 160–175 eV, 22%; and 130–160 eV, 22%. This implies a considerable share of

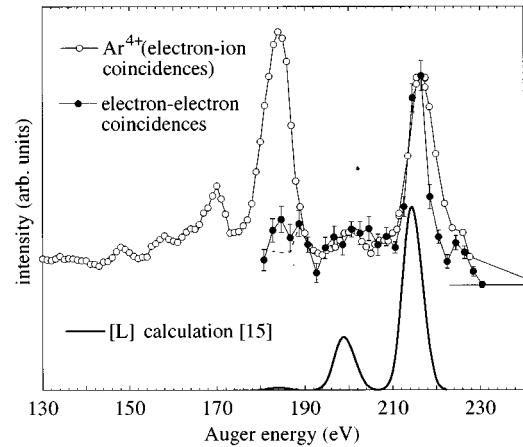


FIG. 8.  $L_{23}$ - $MM$  Auger spectrum observed in coincidence with electrons of  $184.5 \pm 5$  eV. For comparison also the calculated  $[L_{23}]$  vacancy satellite spectrum [16] [cf. Fig. 4(c)] is displayed.

correlation satellites, which actually is even larger since we have no data below 130 eV.

Like we have looked with electron-electron coincidences for successor transitions of the  $2p^4(^1D_2)-2p^53p^4$  ones, we can search for the precursors of the  $2p^53p^4-3p^2$  (i.e.,  $L_{23}[M_{23}^2]-M_{23}M_{23}[M_{23}^2]$ ) lines around 185 eV. To this end we set the 10-eV-wide bandpass of the ESA spectrometer for maximum noncoincident signal of this group. This puts the center of the coincidence window at  $184.5 \pm 2$  eV. The 4-eV bandpass of the other electron spectrometer is stepped from 180 to 230 eV. As can be taken from Fig. 4(b), the spectral intensity falling into the coincidence window comes mostly from transitions leading to  $\text{Ar}^{4+}$  (i.e.,  $L_{23}[M_{23}^2]-M_{23}M_{23}[M_{23}^2]$  lines), but other spectra make noticeable contributions. Their majority does not cause electron-electron coincidences; however, those leading to  $\text{Ar}^{2+}$  or  $\text{Ar}^{3+}$  are not accompanied by another  $L_{23}$ - $MM$  electron emission, while the second electron belonging to  $\text{Ar}^{6+}$  or  $\text{Ar}^{7+}$  falls below 180 eV. Thus we have to consider only the  $\text{Ar}^{5+}$  intensity inside the coincidence window, which amounts to 24% of the  $\text{Ar}^{4+}$  plus  $\text{Ar}^{5+}$  counts. Into the window fall the high-energy wing of the  $L_{23}[M^3]-M_{23}M_{23}[M^3]$  as well as part of the  $L_{23}[LM]-M_1M_{23}[LM]$  lines, as seen by comparing Figs. 4(b) and 4(c). Precursor lines to the former transitions (i.e.,  $[LM]$  lines), and therefore coincidences, may be expected anywhere between 180 and 230 eV, whereas the  $[M^3]$  lines emitted in sequence to the  $[LM]$  ones in the coincidence window are expected to lie below 180 eV. Hence we estimate that roughly half of the  $\text{Ar}^{5+}$  intensity falling into the coincidence window can contribute to the measured electron-electron coincidence spectrum, and these events will preferentially occur around 206 eV, where the  $\text{Ar}^{5+}$  intensity in Fig. 4(b) shows a maximum.

The electron spectrum coincident with electrons of  $184.5 \pm 5$  eV energy is displayed in Fig. 8, together with the electron- $\text{Ar}^{4+}$  coincidence spectrum and the calculated  $[L_{23}]$  one. Most conspicuous is the peak at 216 eV, which corresponds to the  $2p^4(^1D_2)-2p^53p^4$  transitions. Lying 9.6 eV above the  $2p^4(^1D_2)$  state is the  $2p^4(^1S_0)$  state, which is populated at about 1/7 of the  $^1D_2$  state [4]. Transitions from the  $2p^4(^1S_0)$  level to (some of) the same  $2p^53p^4$  states give

rise to the coincidence peak at 225 eV, whose intensity is about 1/5 of the  $^1D_2$  peak. Thus the coincidence measurement supports the former assignment of pairs of consecutively emitted individual  $[L_{23}]$  and  $[M_{23}^2]$  lines [16]. Roughly between 190 and 210 eV the  $L_{23}[L_{23}]-M_1M_{23}[L_{23}]$  lines are expected according to the calculation, and we have already attributed to them the maximum at 200 eV of the electron-Ar $^{4+}$  coincidences. The electron-electron coincidence spectrum appears rather flat in this region. It reproduces the minimum seen in the electron-Ar $^{4+}$  coincidences at 192 eV, but not the one at 205 eV, which probably is obliterated by the  $[LM]-[M^3]$  coincidences discussed above. We ascribe the electron-electron coincidences between 192 and 205 eV mostly to the  $L_{23}[L_{23}]-M_1M_{23}[L_{23}]$  transitions, in accordance with all other information. The coincidence spectrum of Fig. 8 shows another broad maximum around 185 eV. Here, however, both spectrometers have the same pass energy, thereby doubling the coincidence detection probability. The dashed curve in Fig. 8 gives a roughly corrected intensity in this region. Coincidences seen here are attributed to  $L_{23}[L_{23}]-M_1M_{23}[L_{23}]$  transitions and  $[L_{23}]$  correlation satellites.

Concluding the discussion of the two partial  $L_{23}$ - $MM$  spectra leading to final Ar $^{4+}$  ions, we can state that the electron-ion and electron-electron coincidences have revealed their structure in quite some detail and in good agreement with the calculation. The conditions for the investigation of these spectra are comparatively favorable. They belong to the strongest branch of  $K$  hole decay (the  $K-L_{23}L_{23}$  one). Moreover, the interpretation of the electron-electron coincidence spectra is facilitated by the fact that it was possible to select coincidence windows in which the pertinent partial spectra make by far the dominant contribution. It is precisely this circumstance that allowed also the assignment of individual  $[L_{23}]$  and  $[M_{23}^2]$  transitions [16,22]. Electron-electron coincidence spectra taken with other windows would be more difficult to interpret, at least at the resolution attained here. The general structure of the spectra emitted in the two other  $K-L_iL_k$  cascade branches, i.e., those connected to final charges  $q > 4$ , is predicted by the calculation to be quite similar to those of the  $K-L_{23}L_{23}$  branch. However, the longer the cascades, the more this simple structure is expected to be blurred in reality by shake processes and by configuration interaction, both of which have been neglected in the calculation. Indeed, this is readily apparent in Fig. 4(b). While for electron-Ar $^{5+}$  coincidences the two

$L_{23}[LM]-M_{23}M_{23}[LM]$  and  $L_{23}[M^3]-M_{23}M_{23}[M^3]$  peaks still are well discernible, the smaller  $L_{23}[LM,M^3]-M_1M_{23}[LM,M^3]$  maxima predicted by the calculation almost disappear in the background of shake and correlation satellites. For electron-Ar $^{6+}$  coincidences even the principal  $L_{23}[L_{23}M^2,M^4]-M_{23}M_{23}[L_{23}M^2,M^4]$  maxima rise, but a little above the broad overall distribution. Thus the breakdown of the independent-particle picture, progressing with the number of vacancies, already can be recognized in the general structure of the partial spectra.

#### IV. SUMMARY

The  $L_{23}$ - $MM$  Auger spectrum of argon observed after photoexcitation above the 1s threshold is exceedingly rich in overlapping lines since it is actually a superposition of eight complete  $L_{23}$ - $MM$  spectra, each emitted in the presence of a different configuration of "spectator" vacancies. A full decomposition has been achieved, at an energy resolution of 5 eV largely averaging over transition multiplets, by measuring the spectrum in coincidence with a charge analysis of the final ions. The result is in excellent agreement with a published step-by-step calculation of the deexcitation cascade in single-configuration average approximation, but in addition shows the gross intensity distribution of correlation satellites. The sequential nature of transitions belonging to two different spectator vacancy configurations has been directly demonstrated, for the  $K-L_{23}L_{23}$  cascade branch, by electron-electron coincidence spectroscopy. These data are in accordance with the electron-ion coincidence results and with former assignments of pairs of consecutively emitted lines. Both electron-ion and electron-electron coincidence spectroscopy could, at improved energy resolution, serve to assign individual transitions to the various superposed partial spectra. However, it was shown elsewhere that already the gross spectral decomposition and other available information made it possible to assign in this respect the majority of spectral lines that stand out significantly over the quasicontinuous background at the present level of resolution (0.35 eV).

#### ACKNOWLEDGMENTS

This work was funded by the German Federal Minister for Research and Technology (BMFT) under Contract No. 05 5PDAXI 8 and by the Deutsche Forschungsgemeinschaft via Sonderforschungsbereich 334.

- 
- [1] W. Mehlhorn, in *Atomic Inner-Shell Physics*, edited by B. Crasemann (Plenum, New York, 1985), pp. 119–180.
  - [2] L. O. Werme, T. Bergmark, and K. Siegbahn, *Phys. Scr.* **6**, 141 (1972).
  - [3] L. O. Werme, T. Bergmark, and K. Siegbahn, *Phys. Scr.* **8**, 149 (1973).
  - [4] L. Asplund, P. Kelfve, B. Blomster, H. Siegbahn, and K. Siegbahn, *Phys. Scr.* **16**, 268 (1977).
  - [5] E. J. McGuire, *Phys. Rev. A* **11**, 1180 (1975).
  - [6] K. G. Dyall and F. P. Larkins, *J. Phys. B* **15**, 2793 (1982).
  - [7] J. W. Cooper, S. H. Southworth, M. A. McDonald, and T. LeBrun, *Phys. Rev. A* **50**, 405 (1994).
  - [8] W. Eberhardt, G. Kalkoffen, and C. Kunz, *Phys. Rev. Lett.* **41**, 156 (1978).
  - [9] H. Aksela, S. Aksela, H. Pulkkinen, A. Kivimäki, and O.-P. Sairanen, *Phys. Scr.* **41**, 425 (1990).
  - [10] M. Meyer, E. v. Raven, B. Sonntag, and J. E. Hansen, *Phys. Rev. A* **43**, 177 (1991).
  - [11] J. A. de Gouw, J. van Eck, A. C. Peters, J. van der Weg, and H. G. M. Heideman, *J. Phys. B* **28**, 2127 (1995).

- [12] W. Eberhardt, in *Applications of Synchrotron Radiation*, edited by W. Eberhardt, Springer Series in Surface Sciences Vol. 35 (Springer, Berlin, 1995), pp. 203–262.
- [13] G. S. Brown, M. H. Chen, B. Crasemann, and G. E. Ice, *Phys. Rev. Lett.* **45**, 1937 (1980).
- [14] S. Aksela, E. Kukk, H. Aksela, and S. Svensson, *Phys. Rev. Lett.* **74**, 2917 (1995).
- [15] J. Mursu, H. Aksela, O.-P. Sairanen, A. Kivimäki, E. Nõmmiste, A. Ausmees, S. Svensson, and H. Aksela, *J. Phys. B* **29**, 4387 (1996).
- [16] F. von Busch, J. Doppelfeld, C. Günther, and E. Hartmann, *J. Phys. B* **27**, 2151 (1994).
- [17] S. H. Southworth, M. A. McDonald, T. LeBrun, Y. Azuma, and J. W. Cooper, in *Atomic Physics at High Brilliance Synchrotron Sources*, Proceedings of a Workshop held at Argonne National Laboratory, 1994, edited by G. Berry, P. Cowan, and D. Gemmell (Argonne National Laboratory, Argonne, 1994), p. 205.
- [18] S. H. Southworth, M. A. McDonald, T. LeBrun, and R. D. Deslattes, *Nucl. Instrum. Methods Phys. Res. A* **347**, 499 (1994).
- [19] U. Arp, T. LeBrun, S. H. Southworth, M. A. McDonald, and M. Jung, *Phys. Rev. A* **55**, 4273 (1997).
- [20] U. Arp, J. W. Cooper, T. LeBrun, S. H. Southworth, M. Jung, and M. A. McDonald, *J. Phys. B* **29**, L837 (1996).
- [21] A. G. Kochur and V. L. Sukhorukov, *J. Electron Spectrosc. Relat. Phenom.* **76**, 325 (1995).
- [22] J. Doppelfeld, F. von Busch, U. Kuetsgens, and S. Fritzsche (unpublished).
- [23] P. Staib and U. Dinklage, *J. Phys. E* **10**, 914 (1977).
- [24] U. Alkemper, R. Hörnig, and F. von Busch, *J. Phys. B* **29**, 35 (1996).
- [25] F. P. Larkins, *J. Phys. B* **4**, 1 (1971).
- [26] C. Günther and E. Hartmann, *Nucl. Instrum. Methods Phys. Res. B* **98**, 74 (1995).
- [27] J. Doppelfeld, N. Anders, B. Esser, F. von Busch, H. Scherer, and S. Zinz, *J. Phys. B* **26**, 445 (1993).
- [28] M. H. Chen, B. Crasemann, and H. Mark, *At. Data Nucl. Data Tables* **24**, 13 (1979).